Results in Physics 11 (2018) 984–993

Contents lists available at ScienceDirect

Results in Physics

journal homepage: www.elsevier.com/locate/rinp

Study of ultra-hard materials of the B-C-N-O quaternary system

A. Habanyama[a,*], M. Msikita[a], J. Simfukwe[a,b], G.T. Baliga[a], N.K. Mumba[a], M. Mulenga[a], G. Samukonga[a,c]

[a] Department of Physics, Copperbelt University, P. O. Box 21692, Jambo Drive, Riverside, Kitwe 10101, Zambia
[b] Department of Physics, University of Pretoria, Private Bag X20, Hatfiled, Pretoria 0028, South Africa
[c] Department of Physics, Mukuba University, P. O. Box 20382, Itimpi, Garnerton, Kitwe 10101, Zambia

ARTICLE INFO

Keywords:
Ultra-hard material
Elastic constants
Density functional theory

ABSTRACT

A number of potentially ultra-hard materials are examined using ab-initio methods. Compound phases of varying lattice stoichiometry in the B-C-N-O quaternary system, in the forms, $C_{8-x}B_x$ (x = 1, 2, 3, 4), $C_{7-x}BN_x$ (x = 1, 2, 3) and $C_{6-x}BNO_x$ (x = 1, 2) are proposed as possible ultra-hard materials with useful applications. Cell structures and elastic properties are studied, systematic trends are established. It was determined that C_7B and C_6BN were mechanically and dynamically stable compounds with potential ultra-hard characteristics, C_6BN being the harder of the two. Since diamond is experimentally well understood as an ultra-hard material, we use it as a standard for comparing our results.

Introduction

Most researchers define ultra-hard or super-hard materials as those having Vickers hardness greater than 4000 kg/mm^2, which is about 40 GPa [1]. Vickers hardness in kilograms per square millimetre (kg/mm^2) can be converted to SI units (GPa) by multiplying with the standard gravity (9.80665) to get the hardness in MPa and then divided by 1000 to get GPa. A lot of theoretical and experimental work has been devoted to the search for new ultra-hard materials [1-3].

The hardest naturally occurring material known is diamond. Its Vicker hardness, depending on the chosen crystal face indented and type of diamond, varies from 70 to 140 GPa [4]. The material know to be the second hardest from diamond is boron nitride in the cubic phase (cBN), with a hardness of between 30 and 45 GPa [5] on the Vickers scale. Naturally occurring cBN was discovered relatively recently [6].

Ultra-hard materials generally satisfy the three conditions that, the bond lengths should be short, there should be covalent bonding to a high degree and the bond or electronic density should be high [3]. The hardness of diamond is attributed to its localized electrons in covalent bonds formed by sp^3 bonded carbon atoms with two interpenetrating face-centred cubic lattices shifted by $a/4$ of the lattice parameter, a = 0.357 nm, along each cubic axis hence forming short bonds of length, $d = \frac{\sqrt{3}}{4}a$. Ultra-hard materials can be distinguished into a number of classes including the already synthesized and hypothetical phases [4]. In one class of the ultra-hard materials, we have covalent and partially ionic covalent compounds such as oxides formed by elements from the second and third periods of the periodic table. Stable lattices with short covalent bonds are formed by these materials [4]. In this class we have materials like corundum, which is a crystalline form of aluminium oxide (Al_2O_3). Sapphire and ruby are two primary gem varieties of corundum with some transition metal impurities present. Stishovite is also in this class, it is the high pressure phase of SiO_2 which is very rare on the Earth's surface but is the predominant form of silicon dioxide in the lower mantle. Al and Si are both in period 3 of the periodic table while O is in period 2. Another class consists of covalent compounds including various crystalline and disordered carbon modifications. An example is C_{60} molecules packed together in the dense bulk solid-state form called fullerite [4]. A common feature in all classes of ultra-hard materials is that they include at least one of the four elements, carbon, boron, oxygen and nitrogen [7–9]. Our present work is based on the study of the compound phases in the B-C-N-O quaternary system, as a class of materials.

The value of the bulk modulus of diamond is, B = 443 GPa and that of its shear modulus is, G = 535 GPa [10]; for cubic boron nitride, B = 367 GPa and G = 405 GPa [11]. While there is no one-to-one correspondence between bulk or shear modulus with hardness, there is a trend that the larger the bulk and shear moduli the higher the hardness. Diamond has the largest known values of bulk modulus, shear modulus and hardness. The shear modulus was found to be a better predictor of hardness than bulk modulus, using a compilation of experimental data obtained from different materials [12]. Materials like metals do not follow this trend. This is as a result of their low shear strength [13] due

* Corresponding author. Tel.: +260 963313923.
E-mail address: adrian.habanyama@cbu.ac.zm (A. Habanyama).

https://doi.org/10.1016/j.rinp.2018.10.063
Received 10 July 2018; Received in revised form 26 October 2018; Accepted 31 October 2018
Available online 05 November 2018

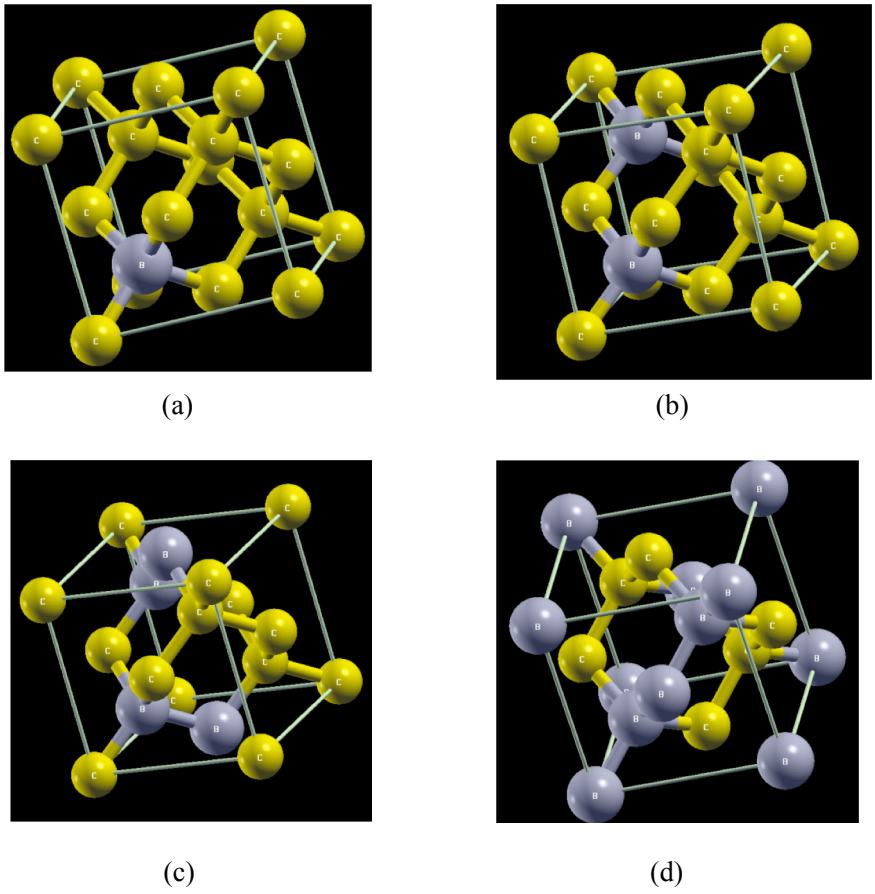

Fig. 1. Unrelaxed unit cell crystal structures of, (a) C_7B, (b) C_3B (or C_6B_2), (c) C_5B_3 and (d) CB (or C_4B_4).

Table 1
Independent stiffness constants, c_{ij} and compliances, s_{ij} for $C_{8-x}B_x$ materials where $x = 0, 1, 2, 3, 4$.

Material	Crystal structure	Stiffness matrix elements, c_{ij} (GPa) and compliance elements, s_{ij} ($\times 10^{-5}$/GPa)									
		c_{11} s_{11}	c_{12} s_{12}	c_{13} s_{13}	c_{14} s_{14}	c_{22} s_{22}	c_{23} s_{23}	c_{33} s_{33}	c_{44} s_{44}	c_{55} s_{55}	c_{66} s_{66}
Diamond	Cubic F (fcc)	1059 95	118 −10						559 179		
C_7B	Cubic I (bcc)	730 158	215 36						473 212		
C_3B	Rhombohedral I	619 199	205 −58	184 −42	−66.1 −47	619 199		613 88	364 291		
C_5B_3	Orthorhombic	470 397	265 −162	269 −162		513 276	137 11	522 272	277 361	357 280	357 280
CB	Orthorhombic	542 216	188 −56	145 −44		608 191	146 −38	523 214	320 313	315 317	316 317

to the 'lubrication' effect of free electrons between atomic planes. Materials with a value of the bulk modulus exceeding 250 GPa are expected to have ultra-hard characteristics [14]. Clerc [15] proposed the electronic factors that determine high bulk moduli in diamond-like materials. In such materials, hardness is known to scale well with the bulk and shear modulus. In our work we start with a diamond-like base structure to predict bulk and other elastic moduli with the aim of identifying novel ultra-hard materials.

The advent of density functional theory (DFT) and ab-initio pseudopotentials has allowed ground state structural and electronic properties calculations as well as predictions of the stability of structural phases in materials. The exchange-correlation energy functional used in this work is the generalized gradient approximation (GGA) [16].

There have been studies reported on the B-C system [17–20], the B-O system [21], B-C-O system [22], B-N-O system [23] and the B-C-N system [24]. We make an extension of this research work by studying structures of varying lattice stoichiometry in the B-C-N-O system in the forms, $C_{8-x}B_x$ ($x = 1, 2, 3, 4$), $C_{7-x}BN_x$ ($x = 1, 2, 3$) and $C_{6-x}BNO_x$ ($x = 1, 2$). The materials were initially simulated in a diamond-like super cell of eight atoms. A relaxation operation was carried out on each of the unit cell structures to allow the atomic positions to self-adjust according to the inter-atomic forces until an equilibrium atomic structure of the system was achieved. Ground-state crystal structures and various moduli of elasticity are examined; systematic trends are established.

Table 2
Effective isotropic Voigt, Reuss and Hill bulk moduli, B, shear moduli, G, Young moduli, E and Poisson ratio, ν.

Material	Crystal structure	B_V and G_V (GPa)	B_R and G_R (GPa)	B_H, G_H and E (GPa)	ν
Diamond	Cubic F (fcc)	$B_V = 432$ $G_V = 523$	$B_R = 432$ $G_R = 520$	$B_H = 432$ $G_H = 522$ $E_H = 1115$	$\nu_H = 0.07$
C_7B	Cubic I (bcc)	$B_V = 386$ $G_V = 387$	$B_R = 386$ $G_R = 354$	$B_H = 386$ $G_H = 370$ $E_H = 842$	$\nu_H = 0.14$
C_3B	Rhombohedral I	$B_V = 333$ $G_V = 272$	$B_R = 333$ $G_R = 242$	$B_H = 333$ $G_H = 257$ $E_H = 613$	$\nu_H = 0.19$
C_5B_3	Orthorhombic	$B_V = 316$ $G_V = 254$	$B_R = 314$ $G_R = 192$	$B_H = 315$ $G_H = 223$ $E_H = 542$	$\nu_H = 0.21$
CB	Orthorhombic	$B_V = 292$ $G_V = 270$	$B_R = 290$ $G_R = 255$	$B_H = 291$ $G_H = 262$ $E_H = 605$	$\nu_H = 0.15$

Computational details

Plane-wave pseudo-potential total energy and electronic structure calculations and simulations were performed using the Quantum Espresso [25] package, based on the density functional theory [26]. The generalized gradient approximation (GGA) [16] was used for the electronic exchange-correlation interactions. In all the calculations, the plane-wave cut-off energy used was 50 Ry and the k-point mesh Brillouin zone sampling was 6 × 6 × 6 Monkhorst Pack [27]. This allowed for a total energy convergence of within one thousandth of an electron-volt per atom.

We consider a unit cell of eight atoms in the diamond lattice structure with B, C, N or O atoms at the lattice points. Both cell parameter and atomic position geometry were optimized using Quantum Espresso [25]. This was done by carrying out a relaxation operation to allow the atomic positions to self-adjust according to the inter-atomic forces thereby achieving equilibrium atomic structures. The equilibrium configurations were then used as reference systems for applying a theoretical strain and observing the associated changes in the total energy. In this way, graphs of the total energy against the imposed strain had minimum positions at the points of zero strain. The Elastic software package [28] was used to calculate second order elastic constants (SOECs) based on the numerical differentiation of the total energy with respect to the associated strain. The stiffness constants, c_{ij} which are components of the stiffness tensor in Voigt notation, were then obtained using,

$$c_{ij} = \frac{1}{V_0}\frac{\partial^2 E}{\partial \eta_i \partial \eta_j}\bigg|_{\eta=0}, \tag{1}$$

where η is the Lagrangian strain and the equilibrium volume is V_0. The components of the stiffness tensor are the proportionality constants connecting the stress tensor components, τ_{ij} to the strain tensor components, η_{ij}. The tensor equation which defines the components, c_{ij} of

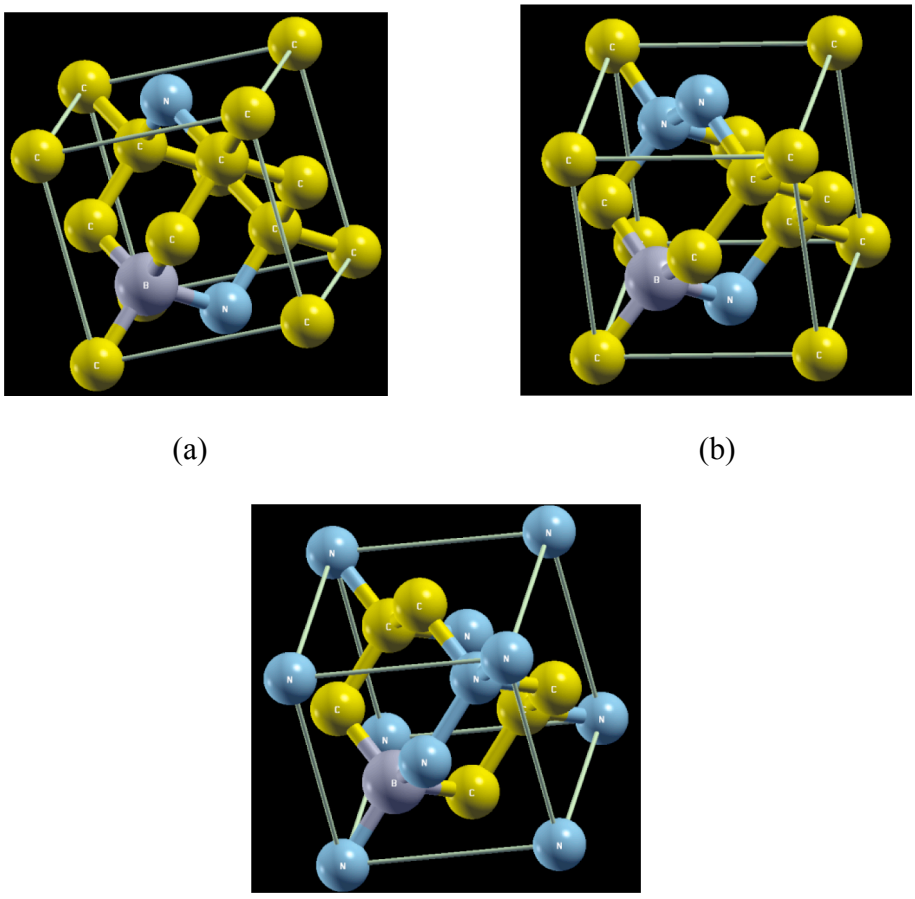

Fig. 2. Unrelaxed crystal structures of, (a) C_6BN, (b) C_5BN_2 and (c) C_4BN_3.

Table 3
Independent stiffness constants, c_{ij} and compliances, s_{ij} for $C_{7-x}BN_x$ materials where $x = 1, 2, 3$.

Material	Crystal structure	Stiffness matrix elements, c_{ij} (GPa) and compliance elements, s_{ij} (1/GPa)													
		c_{11} s_{11}	c_{12} s_{12}	c_{13} s_{13}	c_{14} s_{14}	c_{16} s_{16}	c_{22} s_{22}	c_{23} s_{23}	c_{26} s_{26}	c_{33} s_{36}	c_{36} s_{33}	c_{44} s_{44}	c_{45} s_{45}	c_{55} s_{55}	c_{66} s_{66}
C_6BN	Rhombohedral I	946 108	118 −12	111 −11	−0.5		946 108			975 105		499 200			
C_5BN_2	Monoclinic	770 139	168 −16	148 −9		101 −33	744 240	910 298	115 81	740 −231	−4.4 −91	398 255	45 −30	379 268	378 248
C_4BN_3	Orthorhombic	687 173	156 −32	244 −57			595 183	142 −28		662 178		101 987		367 272	101 987

Table 4
Effective isotropic Voigt, Reuss and Hill bulk moduli, B, shear moduli, G, Young moduli, E and Poisson ratio, ν.

Material	Crystal structure	B_V and G_V (GPa)	B_R and G_R (GPa)	B_H, G_H and E (GPa)	ν
C_6BN	Rhombohedral I	$B_V = 394$ $G_V = 451$	$B_R = 394$ $G_R = 448$	$B_H = 394$ $G_H = 449$ $E_H = 977$	$\nu_H = 0.09$
C_5BN_2	Monoclinic	$B_V = 523$ $G_V = 299$	$B_R = 461$	$B_H = 492$ $E_V = 754$	$\nu_V = 0.26$
C_4BN_3	Orthorhombic	$B_V = 336$ $G_V = 208$	$B_R = 332$ $G_R = 161$	$B_H = 334$ $G_H = 184$ $E_H = 466$	$\nu_H = 0.27$

the stiffness tensor can be inverted to give the components, s_{ij} of the compliance tensor which express the proportionality of η_{ij} to τ_{ij} rather than τ_{ij} to η_{ij}. The effective values of the isotropic shear modulus, G, bulk modulus, B, Young modulus, E and the Poisson ratio, ν, were calculated using the stiffness constants, c_{ij} and compliances, s_{ij}. The bulk modulus was obtained from the ratio of the applied isostatic stress to the fractional volumetric change of the cells. The shear modulus was the calculated resistance to shear stress. The Young modulus related the stress to the resulting strain in the same direction while the Poison ratio related the lateral strain to the axial strain.

There are three widely used averaging approaches for obtaining the isotropic elastic constants. The Voigt [29] approach assumes a uniform strain while the Reuss [30] procedure is valid for uniform stress. The Hill [31] averaging procedure considers the Reuss and Voigt values as the lowest and upper most predicted values respectively.

Bulk and shear moduli in the Voigt approach are given by:

$$B_V = \frac{1}{9}[(c_{11} + c_{22} + c_{33}) + 2(c_{12} + c_{13} + c_{23})] \tag{2}$$

and

$$G_V = \frac{1}{15}[(c_{11} + c_{22} + c_{33}) - (c_{12} + c_{13} + c_{23}) + 3(c_{44} + c_{55} + c_{66})] \tag{3}$$

respectively, while for the Reuss procedure the corresponding expressions are:

$$B_R = [(s_{11} + s_{22} + s_{33}) + 2(s_{12} + s_{13} + s_{23})]^{-1} \tag{4}$$

and

$$G_R = 15[4(s_{11} + s_{22} + s_{33}) - (s_{12} + s_{13} + s_{23}) - 3(s_{44} + s_{55} + s_{66})]^{-1} \tag{5}$$

Hill-averaged bulk and shear moduli were determined using:

$$G_H = \frac{1}{2}(G_V + G_R) \tag{6}$$

and

$$B_H = \frac{1}{2}(B_V + B_R) \tag{7}$$

Hill-averaged Young moduli, E_H, and Poisson ratios, ν_H, were respectively obtained from the expressions:

$$E_H = \frac{9B_H G_H}{3B_H + G_H} \tag{8}$$

and

$$\upsilon_H = \frac{3B_H - 2G_H}{2(3B_H - G_H)} \tag{9}$$

In all the crystal structures, except the monoclinic structures, the Hill-averaged values were used as our final results. In the monoclinic structures, obtaining the Reuss shear modulus, G_R was problematic

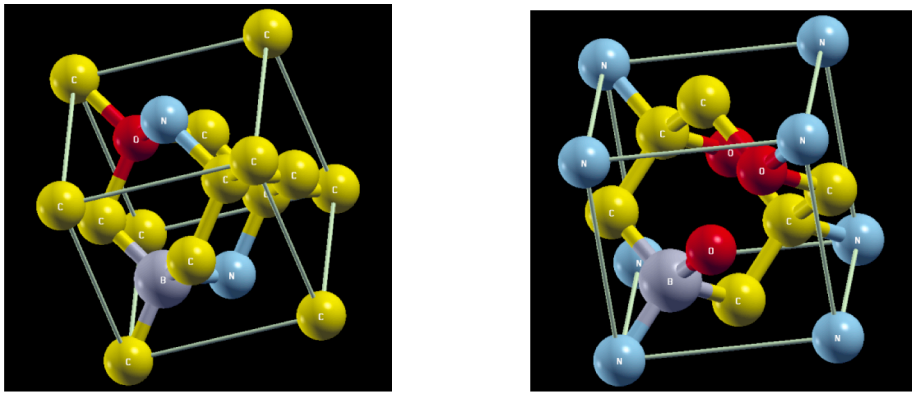

(a) (b)

Fig. 3. Unrelaxed crystal structures of, (a) C_5BNO and (b) C_4BNO_2.

Table 5
Independent stiffness constants, c_{ij} and compliances, s_{ij} for $C_{6-x}BNO_x$ materials where $x = 1, 2$.

Material	Crystal structure	Stiffness matrix elements, c_{ij} (GPa) and compliance elements, s_{ij} (1/GPa)												
		c_{11} s_{11}	c_{12} s_{12}	c_{13} s_{13}	c_{16} s_{16}	c_{22} s_{22}	c_{23} s_{23}	c_{26} s_{26}	c_{33} s_{33}	c_{36} s_{36}	c_{44} s_{44}	c_{45} s_{46}	c_{55} s_{55}	c_{66} s_{66}
C_5BNO	Monoclinic	608 175	185 −2	155 −36	30 −15	709 −379	817 437	107 114	707 −353	9 −132	350 286	−1.4 1	325 308	322 278
C_4BNO_2	Monoclinic	505 231	107 32	190 −98	20 −56	632 406	379 −269	137 −421	557 385	24 251	119 859	−29 75	328 311	119 1287

Table 6
Effective isotropic Voigt, Reuss and Hill bulk moduli, B, shear moduli, G, Young moduli, E and Poisson ratio, ν.

Material	Crystal structure	B_V and G_V (GPa)	B_R (GPa)	B_H, G_H and E (GPa)	ν
C_5BNO	Monoclinic	$B_V = 482$ $G_V = 257$	$B_R = 416$	$B_H = 449$ $E_V = 655$	$\nu_V = 0.27$
C_4BNO_2	Monoclinic	$B_V = 338$ $G_V = 181$	$B_R = 284$	$B_H = 311$ $E_V = 461$	$\nu_V = 0.27$

Table 7
Total equilibrium energies per unit cell for the materials studied.

	Material	Total Equilibrium Energy (Ry)
1	C_4BNO_2	−135
2	C_5BNO	−115
3	C_4BN_3	−111
4	C_5BN_2	−103
5	C_6BN	−94
6	Diamond	−91
7	C_7B	−86
8	C_3B	−81
9	C_5B_3	−75
10	CB	−70

hence the corresponding Young modulus, E_R and Poisson ratio, ν_R, which are derivatives of G_R, could not be determined. In these cases the Voigt rather than the Hill-averaged values were used as the final results.

Results

Diamond and carbon-boride materials were initially simulated in a diamond-like super cell of eight atoms using the formula,

$$C_{8-x}B_x, \quad \text{where } x = 0, 1, 2, 3, 4. \tag{10}$$

The value, $x = 0$ represents diamond which was used as a standard for comparing other possible ultra-hard materials. Crystal structure diagrams were constructed for all the materials, before a relaxation process was carried out, using the crystalline structure visualization and analyzer software package, Xcrysden [32]. Unrelaxed unit cells of C_7B, C_3B (or C_6B_2), C_5B_3 and CB (or C_4B_4) as simulated by Xcrysden are shown in Fig. 1.

The formula in the form, $C_{8-x}B_x$ for a particular value of x is obtainable from the unit cell diagrams in Fig. 1, considering that the atoms at the corners and faces contribute 1/8 and 1/2 of their volume to the cell, respectively. A relaxation operation was carried out on each of the unit cell structures using Quantum Espresso. In this way the atomic positions were allowed to self-adjust according to the interatomic forces until equilibrium of the system was eventually achieved. The Elastic software package [28] was then used to obtain the elastic constants for all the materials. The results are shown in Table 1. The isotropic symmetries of the various second-order elastic constant matrices cause several components to be dependent, for example there is diagonal symmetry in all cases, i.e., $c_{12} = c_{21}$, etc. There are several other types of inter-dependencies like, $c_{11} = c_{22}$ and $c_{66} = (c_{11} - c_{12})/2$, which are characteristic of the rhombohedral I structure. Table 1 only lists the independent elastic constants. It should be noted that the compliance elastic constants were calculated independently of the stiffness constants.

The effective isotropic Voigt, Reuss and Hill values of B, G, E and ν were obtained from the stiffness constants, c_{ij} and compliances, s_{ij}. The results are shown in Table 2.

Nitrogen was then added to the carbon-boride simulated materials using the formula,

$$C_{7-x}BN_x, \quad \text{where } x = 1, 2, 3. \tag{11}$$

Simulated unrelaxed unit cells of C_6BN, C_5BN_2, and C_4BN_3 are shown in Fig. 2.

The systems were then relaxed using Quantum Espresso to obtain equilibrium. The Elastic software package was used to calculate second order elastic constants. In the monoclinic structure, obtaining the Reuss shear modulus, G_R was problematic hence the corresponding Young modulus, E_R and Poisson ratio, ν_R, which are derivatives of G_R, could not be determined. In this case the Voigt rather than the Hill-averaged values were used as the final results as shown in Table 3.

The effective isotropic values of B, G, E and ν were obtained from the stiffness constants and compliances in Table 3, the results are shown in Table 4.

Oxygen was added to the carbon-boron-nitride simulated materials using the formula,

$$C_{6-x}BNO_x, \quad \text{where } x = 1, 2. \tag{12}$$

Unrelaxed unit cells of C_5BNO and C_4BNO_2 as simulated by Xcrysden are shown in Fig. 3.

The Elastic software package was used, after the system was relaxed using Quantum Espresso, to obtain the elastic constants shown in Table 5.

The effective isotropic bulk, shear, Young moduli and Poisson ratio obtained from the stiffness constants and compliances in Table 5 are shown in Table 6.

Both structures in Table 6 are monoclinic and the presented values of B, G, E and ν are the Voigt values.

The total equilibrium energies per unit cell obtained after the relaxation process on all the materials studied are presented in Table 7. C_4BNO_2 has the lowest total energy, the other materials are listed below C_4BNO_2 in Table 7 in their order of increasing equilibrium energy.

Discussion

The variation of the bulk moduli as a function of the values of x in $C_{8-x}B_x$, $C_{7-x}BN_x$, and $C_{6-x}BNO_x$ materials is represented graphically in Fig. 4.

It is seen in Fig. 4(a) that in the $C_{8-x}B_x$ materials the bulk modulus reduces with increasing boron concentration. The trend in the $C_{7-x}BN_x$ materials was not a monotonic reduction with increase in x. We see a jump in the value of the bulk modulus, in Table 3 and Fig. 4(b),

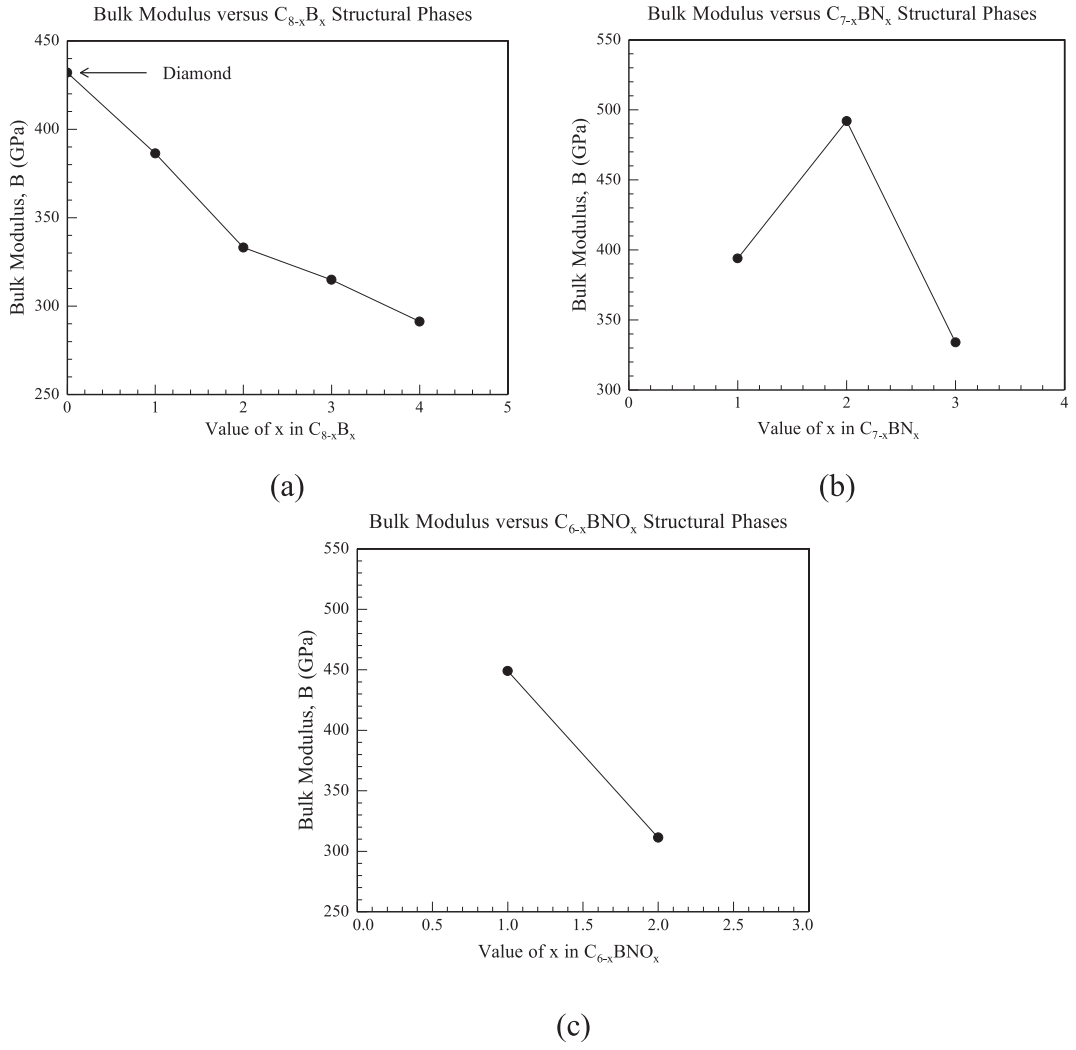

Fig. 4. Graphs for the trend in bulk moduli in, (a) $C_{8-x}B_x$, (b) $C_{7-x}BN_x$, and (c) $C_{6-x}BNO_x$ materials.

associated with the phase change from rhombohedral I to monoclinic in C_6BN and C_5BN_2 respectively. The changes in the shear moduli with variations in lattice stoichiometry are presented in Fig. 5.

Fig. 5(a) shows that there is a graphical minimum in the shear modulus at $x = 3$ (C_5B_3) in the $C_{8-x}B_x$ materials. In the other materials the shear modulus is seen to decrease with increasing values of x. The variations in the Young moduli with changes in lattice stoichiometry are shown in Fig. 6.

As was the case with the shear modulus, we see in Fig. 6(a) that there is a graphical minimum in the Young moduli at $x = 3$ (C_5B_3) in the $C_{8-x}B_x$ materials. In the other materials the Young modulus decreases with increasing values of x. The changes in the Poisson ratio with variations in lattice stoichiometry are presented in Fig. 7.

Fig. 7(a) shows that there is a graphical maximum at $x = 3$ (C_5B_3) in the $C_{8-x}B_x$ materials. The Poisson ratio decreased with increasing values of x in the $C_{7-x}BN_x$ materials but remains constant in the $C_{6-x}BNO_x$ materials.

Table 8 lists the effective isotropic elastic moduli in their decreasing order of magnitude for all materials studied. This table compares the bulk, shear and Young moduli in order to identify the hardest new materials predicted. Materials with a value of the bulk modulus exceeding 250 GPa are expected to have ultra-hard characteristics [14]. The bulk modulus results shown in Table 8 indicate that all the compounds studied could potentially have ultra-characteristics. We shall now discuss the stability of these compounds.

When discussing phase stability, it is important to distinguish between energetic, mechanical and dynamical stability. Energetic stability is related to the Gibbs free energy, G, which predicts the relative stability of compound phases such that the one with the lowest value of G is the most stable one. The Gibbs free energy directly depends on the value of the internal energy, U. The total equilibrium internal energies per unit cell obtained after the relaxation process on all the materials studied are presented in Table 7. The energies in Table 7 are low and it is very likely that the energies required to separate the constituent atoms in the compounds (cohesive or formation energies) are negative, implying energetic stability.

In order to have mechanical stability the elastic constants have to satisfy the Born-Huang conditions [33]. These conditions give simplified equivalents of the generic requirements for the elastic stability of some high-symmetry crystal classes like the cubic system. Mouhat and

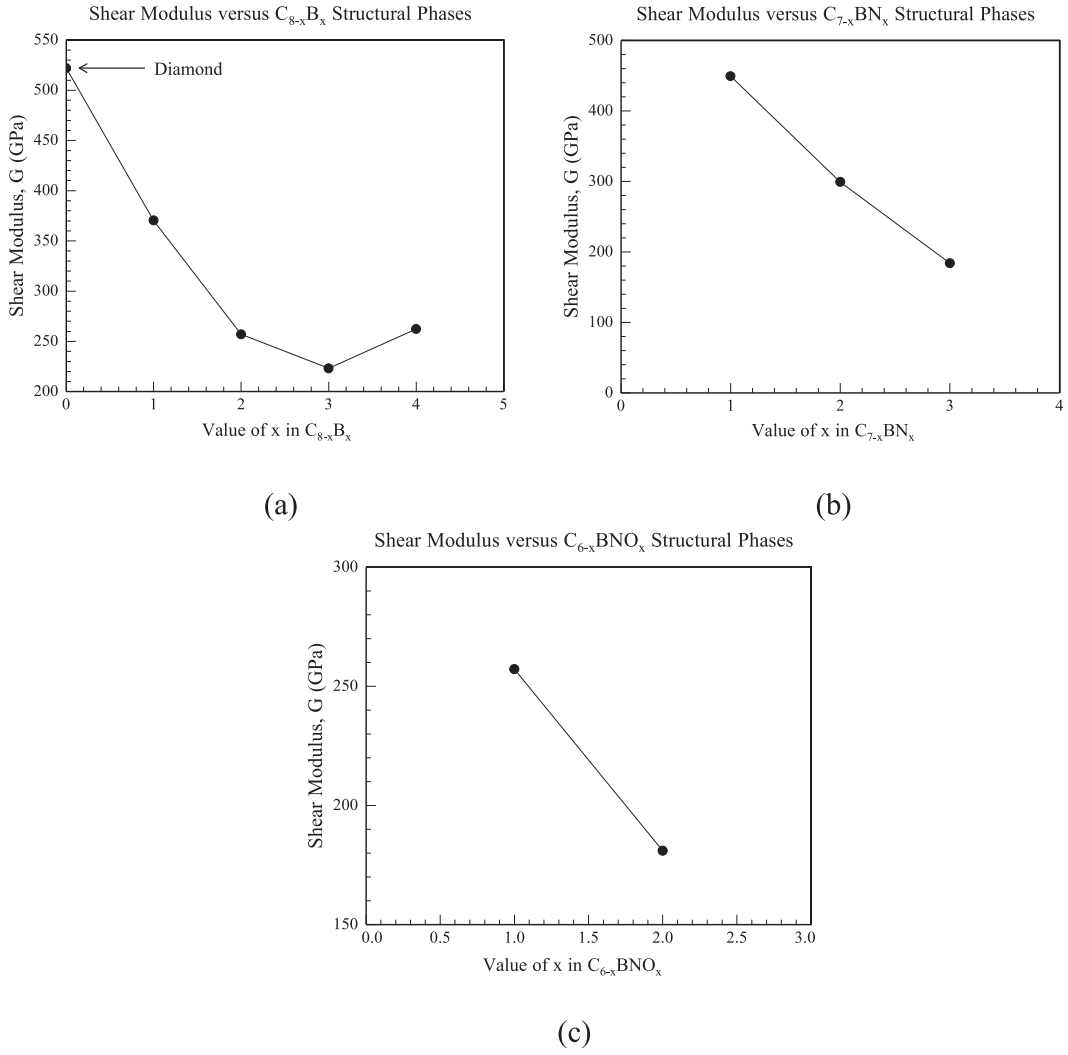

Fig. 5. Graphs for the trend in shear moduli in, (a) $C_{8-x}B_x$, (b) $C_{7-x}BN_x$, and (c) $C_{6-x}BNO_x$ materials.

Coudert [34] extended this work to include both necessary and sufficient conditions for crystal systems with lower symmetry and larger numbers of independent elastic constants. These are the conditions that we adopted in this work.

A general necessary but not sufficient Born stability condition noted by Fedorov [35] is that all diagonal elements should be positive ($C_{ii} > 0, \forall\ i$). An examination of all the diagonal elements in Tables 1, 3 and 5 shows that all the compounds studied satisfy this condition.

Another necessary general Born stability condition is,

$$(C_{ij})^2 < C_{ii}C_{jj}\ \forall\ i, j. \tag{13}$$

An examination of the elastic constants in Tables 1, 3 and 5 also shows that all the compounds studied satisfy the condition in Eq. (13), except in the two cases of C_5BNO for which $C_{23}^2 = 667489$ whereas $C_{22}C_{33} = 501263$ and C_5BN_2 for which $C_{23}^2 = 828100$ whereas $C_{22}C_{33} = 550560$. In both of these cases, $(C_{23})^2 > C_{22}C_{33}$, therefore C_5BNO and C_5BN_2 are not mechanically stable.

The compounds which satisfied the two necessary conditions for mechanical stability were further tested to see if their elastic constants satisfy the sufficient conditions for their respective lattice classes.

The sufficient Born stability conditions for the cubic system, which only has three independent elastic constants, are:

$$C_{11} - C_{12} > 0; \quad C_{11} + 2C_{12} > 0. \tag{14}$$

Using the results shown in Table 1 we see that elastic constants for C_7B, which has a body-centered cubic bravais lattice, satisfy the sufficient Born stability conditions given in Eq. (14). This compound is therefore mechanically stable. Table 1 also shows that the same applies to diamond, as expected, which has a face-centered bravais lattice.

According to Mouhat and Coudert [34] the sufficient Born criteria for the rhombohedral I class, which has 6 independent elastic constants, are:

$$\left.\begin{aligned} &C_{11} > |C_{12}|; \\ &C_{13}^2 < \tfrac{1}{2}C_{33}(C_{11} + C_{12}); \\ &C_{14}^2 < \tfrac{1}{2}C_{44}(C_{11} - C_{12}). \end{aligned}\right\} \tag{15}$$

The elastic constants for C_3B and C_6BN, as presented in Tables 1 and 3 respectively, show that the sufficient Born criteria for these two rhombohedral I compounds, as given in Equation (15), are satisfied.

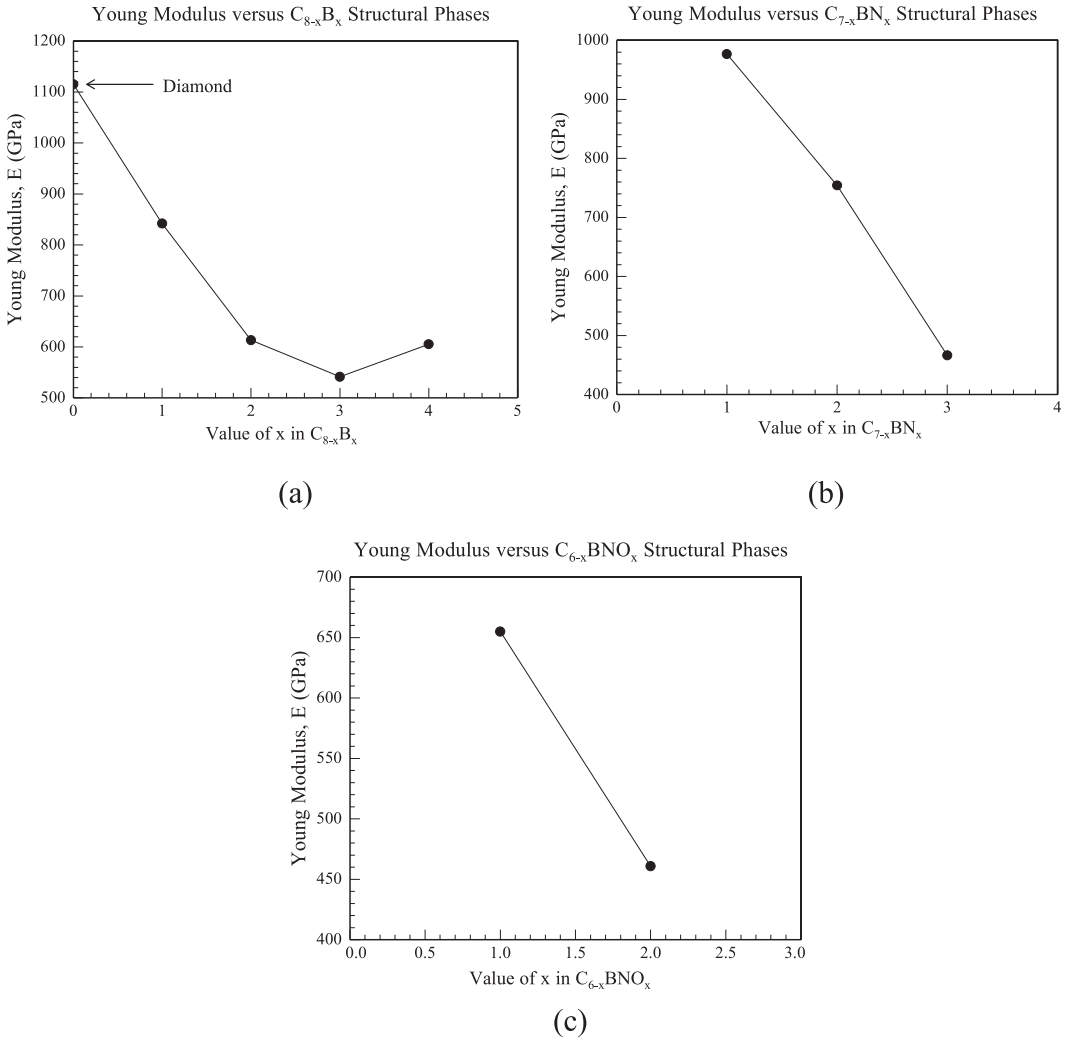

Fig. 6. Graphs for the trend in Young moduli in, (a) $C_{8-x}B_x$, (b) $C_{7-x}BN_x$, and (c) $C_{6-x}BNO_x$ materials.

These two compounds are therefore mechanically stable. It should be pointed out that Tables 1 and 3 show 7 elastic constants for these two compounds as would be the case in rhombohedral II structures. However, this is because our software calculated and presented C_{11} and C_{22} independently while in fact they are always equal, leaving only 6 actual independent constants. The rhombohedral II class has C_{15} as an additional independent elastic constant.

The sufficient Born criterion for an orthorhombic system [34], with 9 independent elastic constants, is:

$$C_{11}C_{22}C_{33} + 2C_{12}C_{13}C_{23} - C_{11}C_{23}^2 - C_{22}C_{13}^2 - C_{33}C_{12}^2 > 0. \quad (16)$$

Using the results shown in Tables 1 and 3, we find that the elastic constants for CB, C_5B_3 and C_4BN_3, which have orthorhombic bravais lattices, satisfy the sufficient Born stability condition given by Eq. (16). These three compounds are therefore mechanically stable.

As demonstrated earlier, of the three monoclinic compounds studied, viz, C_5BN_2, C_5BNO and C_4BNO_2 only C_4BNO_2 satisfied the necessary Born condition given by Equation (14). The monoclinic crystal system has 13 independent elastic constants. The sufficient Born criteria for such low-symmetry crystals are complex [34] and will not be discussed here.

Looking at the bulk, shear and Young modulus values for all the mechanically stable compounds shown in Table 8, none has a higher value of any of the three elastic moduli than diamond; C_5BN_2 and C_5BNO, although predicted as having a higher bulk modulus, have been shown to be mechanically unstable. Interestingly, C_6BN is second to diamond in all the three types of elastic moduli. It is therefore clear that C_6BN is likely to be the hardest of all the mechanically stable compounds studied apart from diamond. The compounds that were identified as being mechanically stable were further tested for dynamical stability. Dynamical stability considers the complete vibrational spectrum of a material: a material is dynamically stable when no imaginary or negative phonon frequencies exist. The Quantum Espresso [25] implementation of Density-Functional Perturbation Theory can be used to calculate phonon frequencies of compounds at a chosen reciprocal lattice vector of the respective Brillouin zones. Our compounds had different lattice structures and hence differently shaped Brillouin zones. The results of our phonon calculations at the center of the Brillouin zones (gamma) are presented in Table 9. This table shows that C_7B and C_6BN have no negative phonon frequencies, the few relatively low frequencies are probably indicative of acoustic mode vibrations while the higher frequencies belong to the optical mode, these materials are

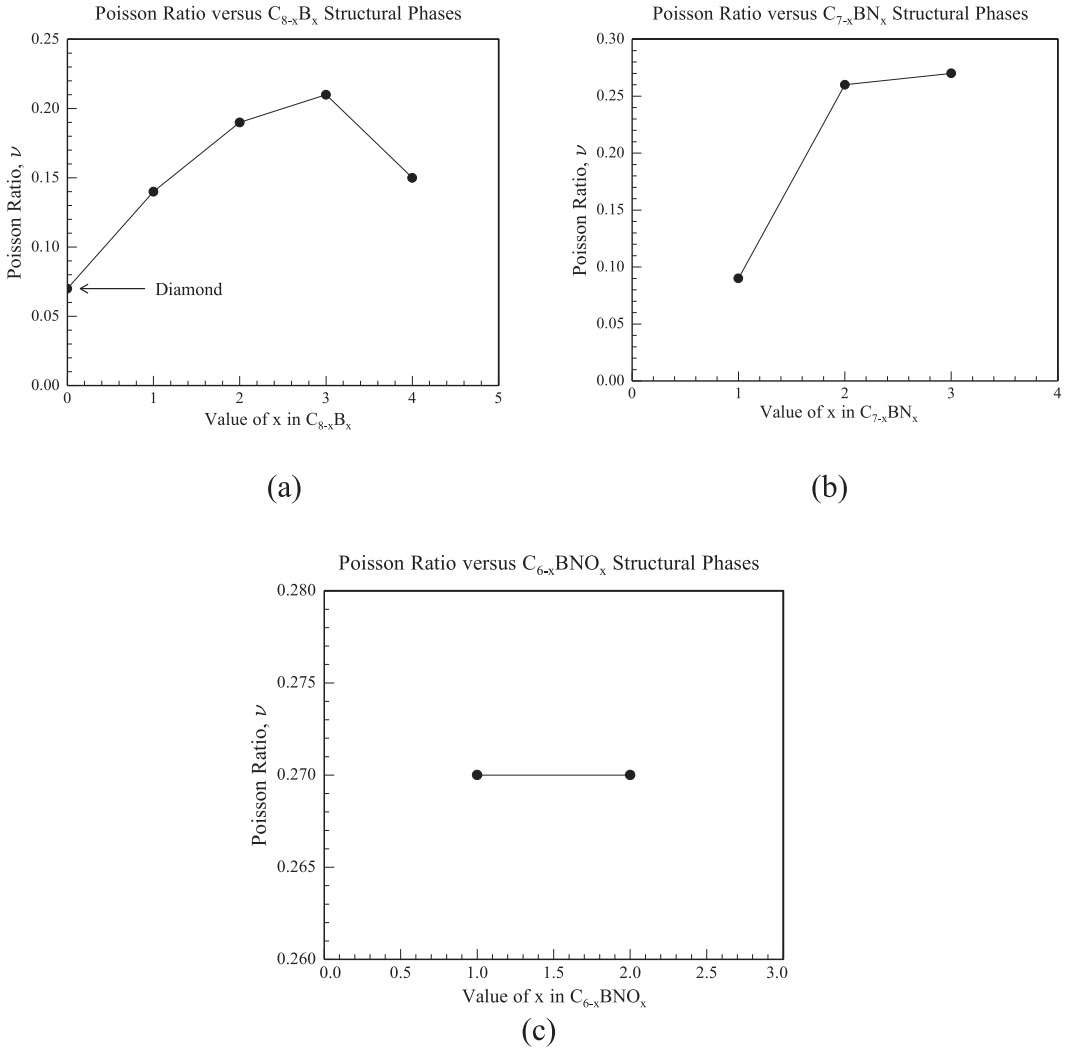

Fig. 7. Graphs for the trend in the Poisson ratio in, (a) $C_{8-x}B_x$, (b) $C_{7-x}BN_x$, and (c) $C_{6-x}BNO_x$ materials.

Table 8
Comparison of bulk, shear and Young moduli for all materials studied.

	Material and bulk modulus, *B* (GPa)		Material and shear modulus, *G* (GPa)		Material and Young modulus, *E* (GPa)	
1	C_5BN_2	492	Diamond	522	Diamond	1115
2	C_5BNO	449	C_6BN	449	C_6BN	977
3	Diamond	432	C_7B	370	C_7B	842
4	C_6BN	394	C_5BN_2	299	C_5BN_2	754
5	C_7B	386	CB	262	C_5BNO	655
6	C_4BN_3	334	C_5BNO	257	C_3B	613
7	C_3B	333	C_3B	257	CB	605
8	C_5B_3	315	C_5B_3	223	C_5B_3	542
9	C_4BNO_2	311	C_4BN_3	184	C_4BN_3	467
10	CB	291	C_4BNO_2	181	C_4BNO_2	461

dynamically stable. Diamond, which was used as a standard for comparison, is also found to be dynamically stable, as expected.

Conclusion

Nine compound phases in the forms, $C_{8-x}B_x$ ($x = 1, 2, 3, 4$), $C_{7-x}BN_x$ ($x = 1, 2, 3$) and $C_{6-x}BNO_x$ ($x = 1, 2$) have been studied as possible ultra-hard materials. On the basis of the bulk modulus results shown in Table 8, all the compounds studied were potentially ultra-hard; their respective values of the bulk modulus exceeding 250 GPa as is expected in ultra-hard materials [14]. However, it was found that C_5BNO and C_5BN_2 were not mechanically stable. It was further determined that of all the mechanically stable compounds only C_7B and C_6BN were also dynamically stable. C_6BN is expected to be the harder of the two based on the results shown in Table 8.

Our results were compared with available results obtained by other researchers using different simulation methods. Nkambule et al. [18] used simulations of molecular dynamics using Tersoff potentials [36] to study some elastic properties of materials in the C-B system with the form, C_xB ($x = 1, 3, 5, 7$). Optimization of the structural geometry and elastic constants were obtained using the GULP package [37]. The materials CB and C_7B were studied in both the molecular dynamics work and our present GGA work. Table 10 compares our results to those of Nkambule et al. In the table, we label the method using molecular dynamics simulation by Nkambule et al. [18] as Tersoff while our method is labeled as GGA. Table 10 shows that there is a general agreement, to within a reasonable simulation error, between the results of the two methods, with a few exceptions.

An area of future study is the investigation of possible ultra-hard

Table 9
Results of phonon calculations, at Γ of the Brillouin zones, for the compounds.

Frequency number	Diamond (cm^{-1})	C_7B (cm^{-1})	C_3B (cm^{-1})	C_6BN (cm^{-1})	CB (cm^{-1})	C_5B_3 (cm^{-1})	C_4BN_3 (cm^{-1})	C_4BNO_2 (cm^{-1})
1	260	179	−−136	73	−83	−120	−101	−84
2	260	179	77	73	−47	−43	−71	−12
3	260	179	112	170	48	61	−47	76
4	824	672	590	712	306	375	412	260
5	824	672	610	712	314	426	454	433
6	824	672	611	735	443	455	562	520
7	824	750	616	772	498	535	581	547
8	824	750	677	774	580	611	701	615
9	824	750	715	774	596	629	721	692
10	1088	779	720	832	619	673	742	697
11	1088	779	808	832	619	687	774	772
12	1088	779	808	970	690	769	784	814
13	1088	978	932	1028	699	776	785	841
14	1088	978	955	1071	708	786	789	892
15	1088	978	963	1071	733	831	922	950
16	1220	1013	1018	1123	821	891	928	960
17	1220	1013	1021	1124	831	900	943	1017
18	1220	1013	1028	1124	880	925	976	1045
19	1220	1061	1043	1200	892	987	1027	1063
20	1220	1061	1052	1200	974	993	1031	1118
21	1220	1102	1079	1207	1151	1065	1085	1124
22	1315	1102	1088	1254	1152	1069	1097	1198
23	1315	1102	1097	1261	1176	1075	1226	1221
24	1315	1112	1099	1261	1187	1075	1376	1262

Table 10
Comparison of results for CB and C_7B obtained by Nkambule et al. [18] using molecular dynamics simulation (Tersoff) to our GGA results.

Material	Method	B (GPa)	G (GPa)	E (GPa)	ν
CB	Tersoff	262	238	494	0.46
	GGA	291	262	605	0.15
C_7B	Tersoff	382	492	910	0.10
	GGA	386	370	842	0.14
Diamond	Tersoff	426	579	1056	0.08
	GGA	432	522	1115	0.07

materials in the B-C-N-O system other than those in the forms, $C_{8-x}B_x$ ($x = 1, 2, 3, 4$), $C_{7-x}BN_x$ ($x = 1, 2, 3$) and $C_{6-x}BNO_x$ ($x = 1, 2$). Fig. 5(a) and 6(a) show a graphical minimum in the G and Y moduli at $x = 3$ (C_5B_3) for the $C_{8-x}B_x$ materials, this indicates that a much higher boron concentration, i.e. with $x > 4$, could substantially increase the hardness of these materials. The work of Nkambule et al. [18] on the C-B system focused on higher carbon rather than boron concentration, i.e. C_xB ($x = 1, 3, 5, 7$).

Acknowledgement

The authors would like to thank the Department of Physics at the Copperbelt University for the use of its institutional facilities.

References

[1] Xu B, Tian YJ. Sci China Mater 2015;58:132.
[2] Li Q, Wang H, Ma Y. J Superhard Mater 2010;32:192.
[3] Tian Y, Xu B, Zhao Z. Int J Refract Met Hard Mater 2012;33:93.
[4] Brazhkin VV, Lyapin AG, Hemley RJ. Philos Mag A 2002;82:231.
[5] Harris TK, Brookes EJ, Taylor CJ. Int J Refract Met Hard Mater 2004;22:105.
[6] Dobrzhinetskaya LF, Wirth R, Yang J, Hutcheon ID, Weber PK, Green HW. High-pressure highly reduced nitrides and oxides from chromitite of a Tibetan ophiolite. PNAS 2009;106:19233.
[7] Zhang M, Liu H, Li Q, Gao B, Wang Y, Li H, et al. Phys Rev Lett 2015;114:015502.
[8] Zinin P, Ming L, Ishii H, Jia R, Acosta T, Hellebrand E. J Appl Phys 2012;111:114905.
[9] Li Q, Chen W, Xia Y, Liu Y, Wang H, Wang H, et al. Diamond Relat Mater 2011;20:501.
[10] Cohen ML. Annu Rev Mater Sci 2000;30:1.
[11] Gao F, He J, Wu E, Liu S, Yu D, Li D, et al. Phys Rev Lett 2003;91:015502.
[12] Hebbache M. Solid State Commun 2000;113:427.
[13] Léger JM, Djemia P, Ganot F, Haines J, Pereira AS, Da Jornada JAH. Appl Phys Lett 2001;79:2169.
[14] Lowther JE. Phys Stat Sol (b) 2000;217:533.
[15] Clerc DG. J Phys Chem Sol 1999;60:103.
[16] Perdew JP, Burke K, Ernezerhof M. Phys Rev Lett 1996;77:3865.
[17] Zhou Dan, Zhao Jiashi, Shen Bingjun, Ying Xu, Zou Yonggang, Tian Jian. Comput Mater Sci 2018;147:238.
[18] Nkambule SM, Lowther JE. Solid State Commun 2010;150:133.
[19] Li QA, Wang H, Tian YJ, et al. J Appl Phys 2010;108:023507.
[20] Liu HY, Li QA, Zhu L, et al. Phys Lett A 2011;375:771.
[21] Li Q, Chen WJ, Xia Y, et al. Diamond Relat Mater 2011;20:501.
[22] Li Y, Li Q, Ma Y, et al. Europhys Lett 2011;95:66006.
[23] Li Qian, Wang Jianyun, Zhang Miao, Li Quan, Ma Yanming. R Soc Chem (RSC) Adv 2015;5:35882.
[24] Shao X. Chin Phys Lett 2011;28:057101.
[25] Giannozzi P, Baroni S, Bonini N, Calandra M, Car R, Cavazzoni C, et al. J Phys: Condens Matter 2009;21:395502.
[26] Kohn W, Sham LJ. Phys Rev 1965;140:A1133.
[27] Monkhorst HJ, Pack JD. Phys Rev B 1976;13:5188.
[28] Golesorkhtabar R, Pavone P, Spitaler J, Puschnig P, Draxl C. Comput Phys Commun 2013;184:1861.
[29] Voigt W. Lehrbuch der Kristallphysik. B. G. Teubner; 1928.
[30] Reuss A, Angew Z. Berchung der Fließgrenze von Mischkristallen auf Grund der Plastizitätsbedingung für Einkristalle. Math Mech 1929;9:49.
[31] Hill R. Elastic properties of reinforced solids: some theoretical principles. J Mech Phys Solids 1963;11:357.
[32] Kokalj A. Comput Mater Sci 2003;28:155.
[33] Born M, Huang K. Dynamics theory of crystal lattices. Oxford University Press; 1954.
[34] Mouhat Félix, Coudert Francois-Xavier. Phys Rev B 2014;90:224104.
[35] Fedorov FI. Theory of elastic waves in crystals. Springer Science + Business Media 1968.
[36] Tersoff J. Phys Rev Lett 1988;61:632.
[37] Gale JD. J Chem Soc Faraday Trans 1997;1:629.